Neodymium Photoluminescence in Whispering Gallery Modes of Toroidal Microcavities

Fedja Orucevic, Jean Hare, Valérie Lefèvre-Seguin

Neodymium Photoluminescence in Whispering Gallery Modes of Toroidal Microcavities

Fedja Orucevic, Jean Hare and Valérie Lefèvre-Seguin

Laboratoire Kastler Brossel – École normale suprieure; UPMC; CNRS
24 rue Lhomond, F-75231 Paris Cedex 05, France

ABSTRACT

Keywords: Microcavity, Microtoroid, Low Threshold Laser, Neodymium, Cavity Quantum Electrodynamics, Optoelectronics

1. INTRODUCTION

The pioneering studies on the interaction between an electromagnetic field and its surrounding environment were conducted by Purcell in 1946[1] and Casimir in 1948.[2] Since then this field of physics has drawn growing interest in both fundamental physics and applications. In the past three decades the use of optical microcavities in the domains such as cavity quantum electrodynamics (CQED),[3] non-linear optics, quantum states engineering, etc. led to numerous experiments that enhanced the comprehension of quantum physics and its fundamental concepts such as decoherence,[4,5] entanglement,[6,7] quantum non demolition measurement (QND),[8] etc.

The apparition of semiconductor microcavities allowed to reproduce those results in the optical domain as required for applied devices.[9] These cavities, generally obtained from MBE grown III-V heterostructures by suitable etching, are mostly of three kinds, named after their shape as micropillars (Fabry-Perot cavities with Bragg reflectors with lateral confinement Total Internal Reflections), photonic crystals (achieving light confinement by 2D or 3D Bragg reflection), and microdisks, using whispering-gallery modes (described below). These cavities generally achieve very good spatial confinement, with mode volumes close to the fundamental limit of $(\lambda/N)^3$ (where λ is the vacuum wavelength and N the refractive index), and their quality factors have been increased progressively from a few hundred to more than tens of thousands, still limited by surface roughness resulting from the etching process. Semiconductor technologies used in fabrication of these cavities make them ideal candidates for integrated optoelectronic devices.

Alternatively, dielectric optical microcavities, such as fused silica microcavities have also been studied as they achieve very high quality factors (up to 10^{10}). They can have different shapes (spherical, cylindrical, toroidal...) but the presence of revolution symmetry allow them to support the so called "Whispering Gallery Modes" (WGM) resulting from light guiding below the curved surface by successive Total Internal Reflections (TIR) at grazing incidence. The very high quality factors of WGM, as high as 10^{10}, as measured in Ref. 10,11, 12 and 13, result from the intrinsic high transparency of the silica and very small surface roughness. Combined with small modal volumes (few hundreds of $(\lambda/N)^3$), they lead to unequalled Q/V ratio and make these cavities perfectly suited for low scale, low threshold lasers and non-linear optical devices.

The coupling between dielectric cavities and different kind of emitters has been extensively studied and reported in the previous works.[14,15] Using the electrical dipole approximation, in the weak coupling regime the rate of spontaneous emission is given by Fermi golden rule as $\Gamma \propto \rho(\omega) \left|\mathbf{d} \cdot \mathbf{E}(\omega)\right|^2$, where $\rho(\omega)$ stands for electromagnetic mode density, $\mathbf{d}$ for dipole strength and $\mathbf{E}(\omega)$ for electrical field. Therefore, the most efficient

Corresponding author Fedja.Orucevic@lkb.ens.fr

This paper was published in "Optoelectronic Devices: Physics, Fabrication, and Application III", *Proceedings of SPIE*, Vol. 6368 (2006) and is made available as an electronic reprint with permission of SPIE.

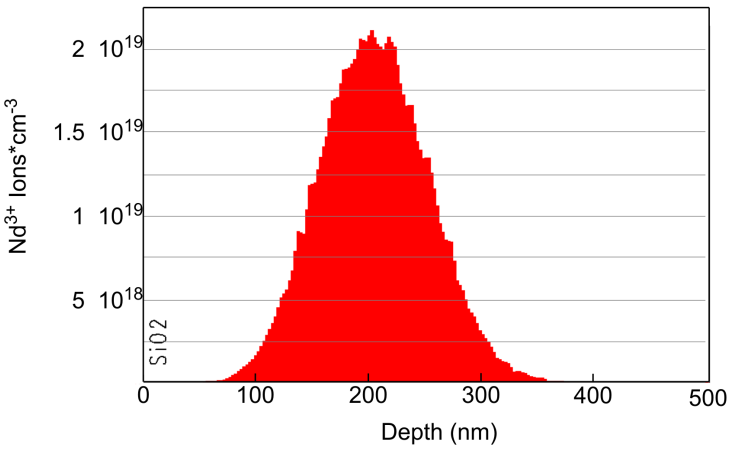

Figure 1. th distribution of implanted Nd^{3+} ions as calculated with SRIM tware. The maximum density of Nd^{3+} ions occurs at the depth of nm and FWHF is about 110 nm.

coupling can be achieved with great dipole emitters placed in the region of maximal electric field. Alkali atoms (namely rubidium or cesium atoms) and semiconductor heterostructures (InAs/GaAs self-assembled quantum dots), have large dipoles (1-10 atom units) but cannot be embedded inside the silica matrix where the WGM field reaches its maximum. However, they can be coupled to WGM using the evanescent wave.[16]

In this work we used the microtoroidal cavities, first introduced by Vahala and co-workers.[17] They are obtained by the laser fusion of silica microdiscs and combine the advantages of easier microdisks integration on silicon substrates and higher Q/V ratios of dielectric fused silica cavities. We used the neodymium ions because they can be easily embedded in the silica matrix by using ionic implantation technique. Despite their small dipole ($d \sim 10^{-2}\, ea_0$) and the large phonon induced homogenous broadening (at room temperature), the coupling of a large number of Nd ions with the maximum electric field, allows to easily observe cavity effects.

2. FABRICATION OF MICROTOROIDS

Fabrication of microtoroids is a two-step process involving successively silicon microelectronic technology and CO_2 laser fusion of silica. In the first step a 800 nm thick layer of silica is produced by thermal oxydation of a silicon substrate. Then silica is bombarded with 600 keV-Nd^{3+}-ions with fluency of $2.5 \cdot 10^{14}$ ions $\cdot$ cm^{-2}. The distribution of Nd^{3+} ions in matrix is calculated using SRIM software[18,19] and yields quasi-gaussian concentration distribution shape with the peak of $2 \cdot 10^{19}$ ions $\cdot$ cm^{-3} at the depth of 200 nm (Fig.1). The limited power of the accelerator did not allow to reach the depth of 400 nm (i.e. the center of the silica layer) where the maximum WMG field is expected. However, the large width of neodymium ion distribution still permitted very good coupling with WGMs (see subsequent paragraphs). After implantation, circular photoresist pads produced by optical or e-beam lithography are transferred to the silica layer by wet etching in buffered HF. The edge of the resulting silica disk is then isolated from the substrate by SF_6/O_2 selective isotropic etching.

In the second step we use CO_2 laser to irradiate the microdisks. As silicon pillar acts as a very efficient thermal sink * in the center of the microdisk the resulting radial temperature gradient leads to fusion of silica only on the microdisk's edges. Surface tension acting on the molten material gives the final toroidal shape of these microcavities (Fig.2-a). Using a fast camera (1000 fps) we observed the dynamics of the microtoroids' formation. The fusion process leads to the final shape of microtoroid in less than 10 ms (Fig.2-b). Using the cylindrical symmetry, we easily modeled heat transfer process in microdiscs. Dimensions of the microdiscs that we used (typically, diameter $d = 100\,\mu$m and disc thickness $t = 800\,$nm) lead to very short characteristic times of

*The temperature varies less than 100 K between top side, in contact with silica, and bottom side, in contact with silicon substrate acting as thermostat.

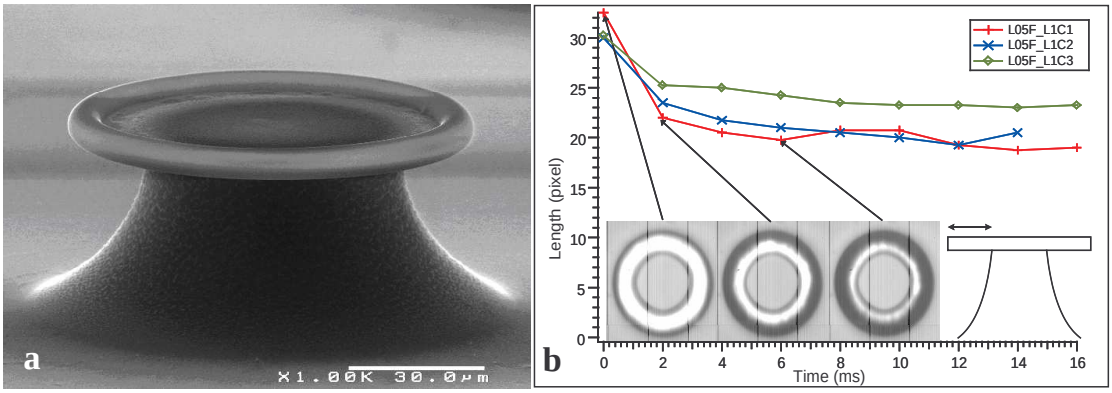

Figure 2. **a** — SEM image of a pure silica 90 μm diameter microtoroid. **b** — The curves show the undercut length of a several microdiscs as a function of irradiation time. The undercut is defined as depicted by the double arrow on the schema at the bottom right corner of the figure. In the inlet are shown three images of a given microdisc at three different times of fusion process (0 ms, 2 ms and 6 ms).

heat diffusion through silica ($\tau_{SiO_2} = 8\,\mu$s) and silicon ($\tau_{Si} = 25\,\mu$s) that are much smaller than the microtoroids' formation time. Therefore the Fourier time-dependant heat transfer equation is recast in a Poisson-like steady-regime equation that we resolved using a standard over-relaxation method.

The formation of a microtoroid is an auto-regulated process: the molten silica reflow toward center until the temperature of the microtoroid's edge reach the fusion point. Thus, the CO_2 laser power and the geometry of microdiscs solely determine the temperature gradient and hence the final shape of a microtoroid, as far as the duration of the laser shot is greater than the time required to form the microtoroid ($\simeq 10$ ms).

The pillars of Nd^{3+} implanted microdiscs had not the perfect cylindrical symmetry, but presented a square-like shape on the top side in contact with the silica microdiscs. That could be the result of the Si/SiO_2 contact interface as the pillars are etched preferentially over the two Si crystal axis. Thanks to the basics properties of heat diffusion, the temperature distribution which is square-shaped on the pillars becomes more circular further from the center. We managed to stop the formation of microtoroid before it approached the pillars too much by controlling the CO_2-laser pulse via a computer generated TTL gate. The succession of short manually triggered 1 ms-pulses allowed to control distance between toroid edge and the pillar.

3. EXPERIMENTAL PROCEDURE

We pumped neodymium ions by a tightly focused laser on edge of microtoroid ($\lambda = 532$ nm, pump waist $\simeq 3\,\mu$m, $P = 9$ mW). This enhances the detection contrast between WGM confined near the microtoroid's edge and leaky modes located in the whole volume of microtoroid.

We first performed the collection of light scattered from a microtoroid using a cleaved multimode optical fiber placed about 100 μm apart from it. The spectrum of the scattered light does not exhibit resonances but matches the PL spectrum of neodymium ions embedded in bulk silica. Indeed, most of Nd^{3+} ions are not coupled to the WGMs but rather emit in the leaky modes of the cavity and the large numerical aperture fiber ($NA \simeq 0.22$) placed in the far field collects light originating from the large portion of the microtoroid. In a previous work,[20] a microscope objective allowed to selectively detect light coming from the edge of erbium doped microtoroids, thus leading to observe the WGM emission spectrum.

Here, we chose to perform this selective detection by a near field method. This was done by evanescent wave coupling between the microtoroid and an angle polished multi-mode fiber.[21] The angle of polishing Φ is chosen

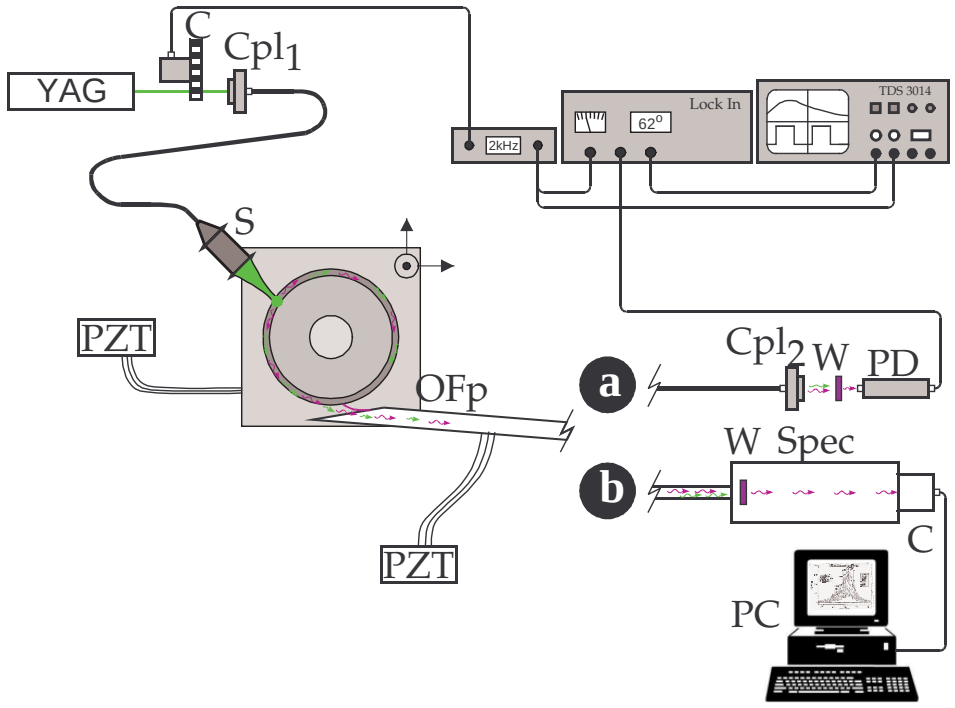

Figure 3. Sketch of experimental setup. The pump laser is a doubled YAG ($\lambda = 532\,\mathrm{nm}$), coupled ($\mathrm{Cpl}_1$) into the singlemode fiber. A system (S) of two lenses is used to focus the laser beam to a spot of $6\,\mu\mathrm{m}$ in diameter. PL signal from the Nd^{3+} embedded ions is collected with the polished fibre ($\mathrm{OF_p}$). **Path a** – PL is collimated by coupler (Cpl_2) to the photodiode (PD) through a 850 nm cut-off filter (W) to remove the residual pump light. **Path b** – After optimisation, the PL is sent through the spectrograph's slits. A 850 nm cut-off filter (W) is placed inside the spectrograph (Spec) and the signal is recorded with the spectroscopic camera (C).

to fulfill the phase-matching requirement for WGMs:

$$\Phi = \arcsin\left(\frac{N_{\mathrm{eff}}}{N_{\mathrm{f}}}\right), \tag{1}$$

where N_{f} is the fiber core index and N_{eff} the effective index of the microtoroid's WGM, that can be estimated from the semiclassical equation for a sphere:

$$Nx = \ell + \frac{1}{2} + \left(\frac{\ell+1}{2}\right)^{1/3} \alpha_n + \cdots \tag{2}$$

Here N is the refractive index of silica, $x = 2\pi a/\lambda$ the size parameter, where a is the radius of the sphere, ℓ is the quantum angular number and α_n are the successive zeros of $Ai(-z)$ (Airy function). For large size parameters ($\ell \gg 1$) and low order WGMs (n close to 1), the internal caustic is close to the surface and we can substitute $\ell \simeq Nx$ in the equation (2) to obtain:

$$N_{\mathrm{eff}} \equiv \frac{\ell}{x} \approx N\left[1 - \frac{2^{-1/3}}{(Nx)^{2/3}}\,\alpha_n\right]. \tag{3}$$

For a microtoroid's diameter of $50\,\mu\mathrm{m}$ and for the $n = 1$ radial order WGM the angle is $\Phi \simeq 18°$. As the microtoroids hold on pillars of $20 - 30\,\mu\mathrm{m}$ in height from silicon substrate, one needs to use a fiber with suitable core and cladding diameters, i.e. $(d_{\mathrm{cl}} - d_{\mathrm{co}})/2 < h_{\mathrm{p}}$. Here d_{cl} and d_{co} are the diameters of, respectively, the

optical cladding and the fiber core, while h_p is the height of a pillar. In our experiment we used a fiber with $d_{co} = 100\,\mu$m, $d_{cl} = 110\,\mu$m and NA = 0.22 (Newport F–MCB–T).

Fig. 3-a shows the experimental setup used to optimise the PL signal. Two sheets (W) of 850 nm cut-off filter (Wratten 87C) remove residual pump light before the signal reaches a Si-photodiode (PD). To extract the PL signal from the noise, the pump beam was chopped (C) at a frequency of about 2.5 kHz and a lock-in amplifier was used. Finally, the signal is monitored on the oscilloscope and optimised using PZT to control the position of laser spot and the gap between the microtoroid and the fiber. Then, the signal analysed with a grating spectrograph (Acton SpectraPro 300i, 1200 grooves/mm) is accumulated for 10 min on a cooled spectroscopic camera (Princeton Instruments SpectruMM 120) as shown in the Fig. 3-b.

4. RESULTS AND DISCUSSION

The expected Free Spectral Range (FSR) of WGM in the microtoroids (and more generally, any other cylindrical symmetry cavity) is given by

$$\Delta\lambda_{FSR} = \frac{\lambda^2}{2\pi\, a\, N_{eff}}, \tag{4}$$

where a is the microtoroid's great radius, N_{eff} is the effective index as obtained in eq. 3 and λ is the vacuum wavelength. Fig. 4 shows PL spectra obtained from a microtoroid of about 55 μm in diameter (measured with standard optical microscope). The different curves correspond to different values of the gap between the fiber and the microtoroid. We identify a FSR of about 3.2 nm, as expected from equation 4 for 55 μm diameter

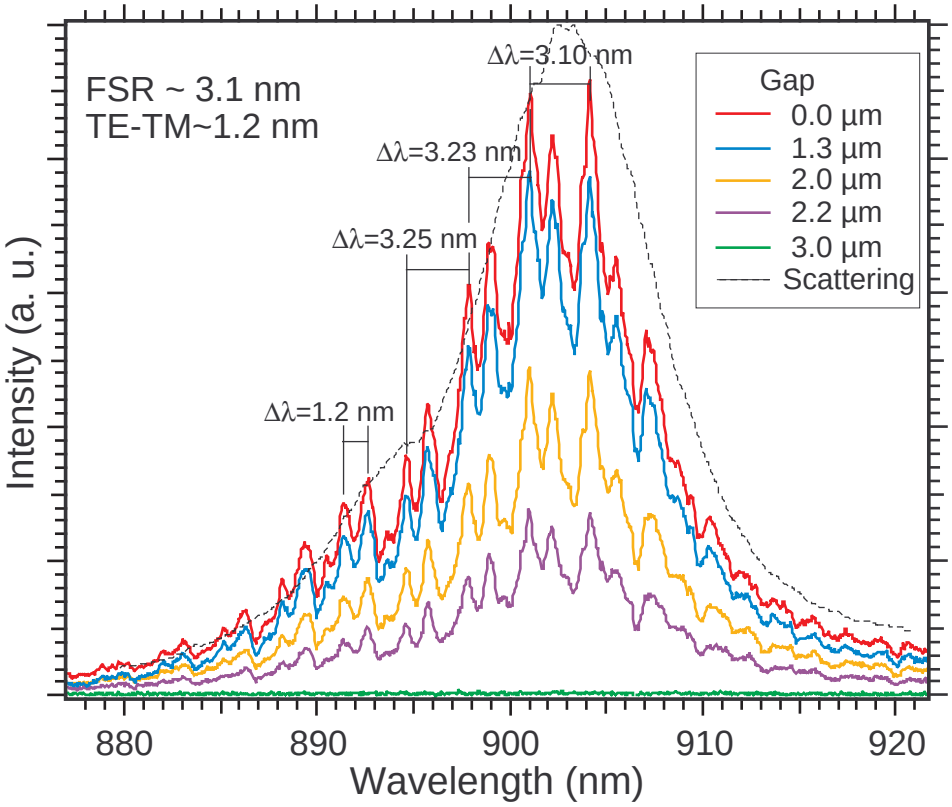

Figure 4. PL spectra from a Nd^{3+} doped 55 μm diameter microtoroid. The dotted curve is the PL spectrum of scattered light from the Nd^{3+} ions. Other curves are the PL spectra obtained by coupling the evanescent wave. Two frequency intervals of 3.2 nm and 1.2 nm correspond, respectively, to the cavity FSR and TE-TM frequency splitting.

microtoroids. The frequency interval of about 1.2 nm corresponds to the TE-TM polarisation splitting. The signal strength is maximum when the fiber is in contact with microtoroid and disappears at 3 μm gap.

The ultimate spectrograph resolution of 0.1 nm restrains us from measuring quality factors higher than a few thousands, while we expect values in the range of $10^8 - 10^{10}$.[17] Furthermore, as the fiber core diameter (80 μm) is very large compared to the thickness of the microtoroid (a few micrometers), it is very likely that several WGMs are coupled in the fiber at once. Those factors contribute to the broadening of the peaks observed in the spectrum.

5. PROSPECTS

The peak of neodymium absorption is at 810 nm, so the pump efficiency can be improved using a laser at this wavelength rather than 532 nm. The development of tapered fibre couplers, that we have just achieved, will even allow to inject the pump laser in resonance with a WGM and therefore enhance the luminescence of neodymium ions in the WGMs.

Our next aim is to demonstrate low threshold Nd-microlaser as an integrated version of an earlier reported work on microspheres[22] and the observation of Silicon Rich Oxides (SrO) microtoroids' PL spectrum.

ACKNOWLEDGMENTS

The authors would like to warmly acknowledge Jérémy Verbert, Emmanuel Hadji and Jean-Michel Gérard from SP2M - CEA - Grenoble for very rich and fruitful collaboration and for providing microdiscs samples.

This work has been supported by the "Programme National Nanosciences" (ACI Microtores).

REFERENCES

[1] E. M. Purcell, "Spontaneous emission probabilities at radio frequencies," *Phys. Rev.* **69**, p. 681, 1946.

[2] H. B. G. Casimir and D. Polder, "The influence of retardation on the London-van der Waals forces," *Phys. Rev.* **73**, p. 360, 1948.

[3] S. Haroche, "Cavity quantum electrodynamics," in *Fundamental Systems in Quantum Optics, Les Houches Summer School, Session LIII*, J. Dalibard, J.-M. Raimond, and J. Zinn-Justin, eds., p. 767, North Holland, Amsterdam, 1992.

[4] W. H. Zurek, "Pointer basis of quantum apparatus: Into what mixture does the wave packet collapse?," *Phys. Rev. D* **24**, p. 1516, 1981.

[5] J.-M. Raimond, M. Brune, and S. Haroche, "Reversible decoherence of a mesoscopic superposition of field states," *Phys. Rev. Lett.* **79**, p. 1964, 1997.

[6] S. Haroche, M. Brune, and J.-M. Raimond, "Experiments with single atoms in a cavity: entanglement, schrödinger's cats and decoherence," *Phil. Trans. Roy. Soc* **355**, p. 2367, 1997.

[7] V. Buzek, H. Moya-Cessa, P. L. Knight, and S. D. L. Phoenix, "Schrödinger-cat states in the resonant Jaynes-Cummings model: Collapse and revival of oscillations of the photon-number distribution," *Phys. Rev. A* **45**, p. 8190, 1992.

[8] M. Brune, S. Haroche, V. Lefèvre, J.-M. Raimond, and N. Zagury, "Quantum non-demolition measurements of small photon numbers by Rydberg atoms phase senstive detection," *Phys. Rev. Lett.* **65**, p. 976, 1990.

[9] T. Yoshie, A. Scherer, J. Hendrickson, G. Khitrova, H. M. Gibbs, G. Rupper, C. Ell, O. B. Shchekin, and D. G. Deppe, "Vacuum rabi splitting with a single quantum dot in a photonic crystal nanocavity," *Nature* **432**, p. 200, 2004.

[10] V. B. Braginsky, M. L. Gorodetsky, and V. S. Ilchenko, "Quality-factor and non-linear properties of optical whispering-gallery modes," *Phys. Lett. A* **137**, pp. 393–397, 1989.

[11] L. Collot, V. Lefèvre-Seguin, M. Brune, J. M. Raimond, and S. Haroche, "Very high-Q whispering-gallery mode resonances observed on fused silica microspheres," *Europhys. Lett.* **23**, p. 327, 1993.

[12] M. L. Gorodetsky, A. A. Savchenkov, and V. S. Ilchenko, "Ultimate Q of optical microsphere resonators," *Opt. Lett.* **21**, pp. 453–455, 1996.

[13] D. W. Vernooy, V. S. Ilchenko, H. Mabuchi, E. W. Streed, and H. J. Kimble, "High-Q measurements of fused-silica microspheres in the near infrared," *Opt. Lett.* **23**, pp. 247–249, 1998.

[14] R. K. Chang and A. J. Campillo, eds., *Optical processes in microcavities*, vol. 3 of *Advanced Series in Applied Physics*, World Scientific, 1996.

[15] A. B. Matsko, A. A. Savchenkov, D. Strekalov, V. S. Ilchenko, and L. Maleki, "Review of applications of whispering-gallery mode resonators in photonics and nonlinear optics," *IPN Progress Report 42-162 (http://tmo.jpl.nasa.gov/progress_report/42-162/162D.pdf)* , 2005.

[16] J. Hare, S. Steiner, F. Orucevic, and V. Lefèvre-Seguin, "Silica microspheres as high-Q microcavities for semiconductor quantum-dot lasers," *Optoelectronic Integrated Ctrcuits VII Proc. of SPIE* **Vol. 5729**, p. 94, 2005.

[17] D. K. Armani, T. J. Kippenberg, S. M. Spillane, and K. J. Vahala, "Ultra-high-Q toroid microcavity on a chip," *Nature* **421**, p. 925, 2003.

[18] J. Biersack and L. Haggmark, "A monte carlo computer program for the transport of energetic ions in amorphous targets," *Nucl. Instr. and Meth.* **174**, pp. 257–269, 1980.

[19] J. Ziegler, "The stopping and range of ions in matter," *Nucl. Instr. Meth. B* **216**, pp. 1027–1036, JUN 2004.

[20] J. Verbert, F. Mazen, T. Charvolin, E. Picard, V. Calvo, P. Noé, J. M. Gérard, and E. Hadji, "Efficient coupling of Er-doped silicon-rich oxide to microdisk whispering gallery modes," *Appl. Phys. Lett.* **86**, pp. 111117–1–111117–3, 2005.

[21] V. S. Ilchenko, X. S. Yao, and L. Maleki, "Pigtailing the high-Q microsphere cavity: A simple fiber coupler for optical whispering-gallery modes," *Opt. Lett.* **24**, p. 723, 1999.

[22] V. Sandoghdar, F. Treussart, J. Hare, V. Lefèvre-Seguin, J.-M. Raimond, and S. Haroche, "Very low threshold whispering-gallery mode microsphere laser," *Phys. Rev. A* **54**, p. R1777, 1996.